Investigation of Supersonic Wing Shape Using Busemann Biplane Airfoil (AIAA-2007-0686)

M. Yonezawa,[1] H. Yamashita[2] and S. Obayashi[3]
Tohoku University, Sendai, Japan, 980-8577

and

K. Kusunose[4]
Formerly Tohoku University, Sendai, Japan, 980-8577

Busemann biplane significantly reduces wave drag due to its thickness (or volume) at supersonic speeds using the shock wave interaction between the two wings. This paper investigates the influence of the three-dimensional effect to the rectangular wing using the biplane concept and considers the effects of various wing configurations which are a rectangular wing using a winglet, two tapered wing configurations and a Caret wing configuration based the Waverider concept.

Nomenclature

b	=	semi-span
C_D	=	wave drag coefficient of wing
C_d	=	wave drag coefficient of airfoil (wing section)
C_p	=	pressure coefficient
c	=	chord length
c_{ref}	=	reference chord length
h	=	gap between biplane elements
M_∞	=	free-stream Mach number
t	=	airfoil thickness
x	=	airfoil-chord direction, or free-stream direction
y	=	wing-span direction
z	=	thickness direction
ε	=	wedge angle
α	=	angle of attack

I. Introduction

A fundamental problem preventing commercial transport aircraft from supersonic flight is the creation of strong shock wave, which results in lower aerodynamic efficiency and the creation of a cruise-condition sonic boom felt on the ground. Because the strength of the shock wave generated by an aircraft flying at the supersonic speed is largely related to both its weight and volume, it has been considered impossible to reduce the strength of the shock wave.

In 1930s, Adolf Busemann suggested a zero wave drag airfoil using a biplane concept at supersonic speeds. It is called Busemann biplane[1, 2] and its configuration is shown in Figure 1. The Busemann biplane creates shock waves at the leading edges. The shock wave propagated to ground can be significantly reduced because Busemann biplane cancels out the shock wave due to the airfoil thickness. Recently, the utility of the biplane concept was shown by

[1] Ph. D. Student, Institute of Fluid Science, yonezawa@edge.ifs.tohoku.ac.jp.
[2] Ph. D. Student, Institute of Fluid Science, yama@edge.ifs.tohoku.ac.jp.
[3] Professor, Institute of Fluid Science, obayashi@ifs.tohoku.ac.jp, Associate Fellow AIAA.
[4] Visiting Professor, Currently Ministry of Defense, Tokyo, Japan, 190-8533, kusunose@jda-trdi.go.jp, Member AIAA.

Kusunose *et al.*[3] Those fundamental studies were based on Euler analysis. Figure 2 shows an example of CFD analysis using an Euler solver that is a C_p distribution around the Busemann biplane airfoil.

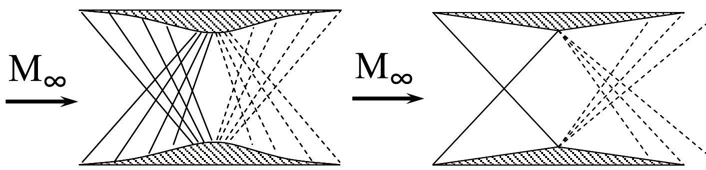

(a) Zero thickness drag. **(b) Small thickness drag.**
Figure 1. Busemann biplane.

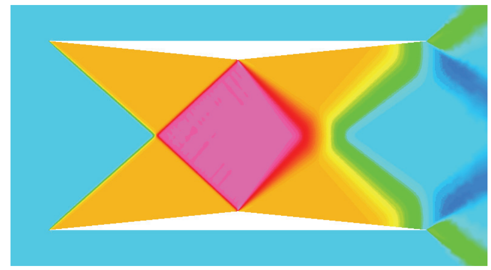

Figure 2. C_p contour plot around Busemann biplane airfoil, M_∞=1.7, α=0 degree.

Here, we consider the wing configurations because it is necessary to investigate the influence of the three-dimensional effect in the wing using the Busemann biplane airfoil in the construction of aircraft. In general, three-dimensional effect is attributable that a Mach wave spreads backward and outward from the aircraft in a cone shape (a so-called Mach cone). A Mach cone is generated by oblique shock wave on the leading-edge of a fuselage (see in Figure 3) and on the wing root, the wing-tip and the kink in a wing (see in Figure 4). In this study, one wing using Busemann biplane airfoil, whose wing planar shape is a rectangle, is analyzed for investigation of the three-dimensional effect. And four other wings using the biplane concept have been considered to find out their shock wave interaction patterns. One is a biplane with a winglet to shut out the wing-tip effect. Others are wings with a taper to reduce the three-dimensional effect. These wings are only analyzed at zero angle of attack.

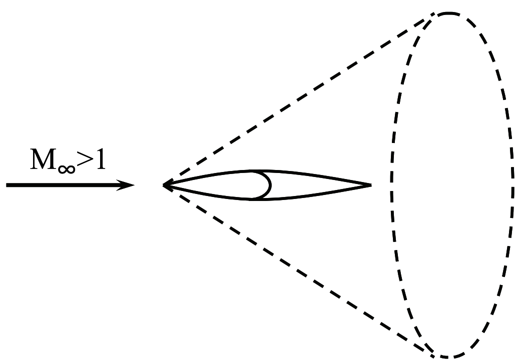

Figure 3. Mach cone on a needlelike body.

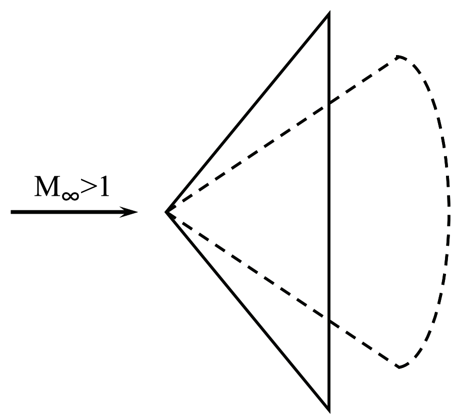

Figure 4. Mach cone on the wing root.

II. Computational Method

In this research, a three-dimensional unstructured flow solver named TAS code (Tohoku University Aerodynamic Simulation code)[4–6] is employed to simulate flow fields. Euler equations are solved by a finite-volume cell-vertex scheme. The numerical flux is computed using the approximate Riemann solver of Harten-Lax-van Leer-Einfeldt-Wada (HLLEW).[7] The second order spatial accuracy is realized by a linear reconstruction of the primitive gas dynamic variables with Venkatakrishnan's limiter. The lower/upper symmetric Gauss-Seidel (LU-SGS) implicit method for unstructured mesh[8] is used for the time integration.

III. Geometry and Flow Condition

The wing sections of all wing configurations in this study are based on the airfoil modified small thickness drag Busemann biplane. This section explains about the airfoil and five wing configurations. These wings are defined with almost same reference area and aspect ratio as the basis of the rectangular wing. They are analyzed at a free-stream Mach number of 1.7 and at the angle of attack of 0 degree.

A. Airfoil of wing sections

The airfoil is a modified configuration of the small thickness drag Bumsenann biplane (see in Figure 1 (b)). The gap of this biplane for ideal shock wave interaction is related to Mach number and thickness-chord ratio. In this study, design Mach number (M_∞) is 1.7 and thickness-chord ratio (t/c) of an airfoil of the biplane is 0.05. Its equivalent wedge angle (ε) is 5.71 degrees. Thus, the gap of the biplane has been adjusted, to have ideal shock wave interaction at non-linear two shock interaction theory (z/c = 0.505). Figure 5 shows the airfoil configuration. In the following wing configurations, this airfoil configuration is used as base wing sections.

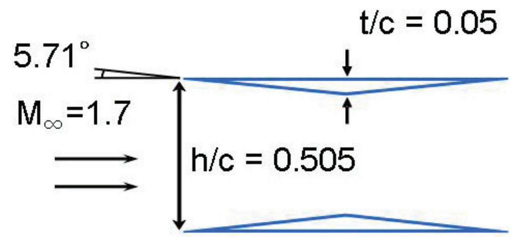

Figure 5. Airfoil configuration using as wing sections.

B. Rectangular wing

The rectangular wing has no sweep, taper, nor dihedral (see in Figure 6). The aspect ratio is 4 (b/c = 2).

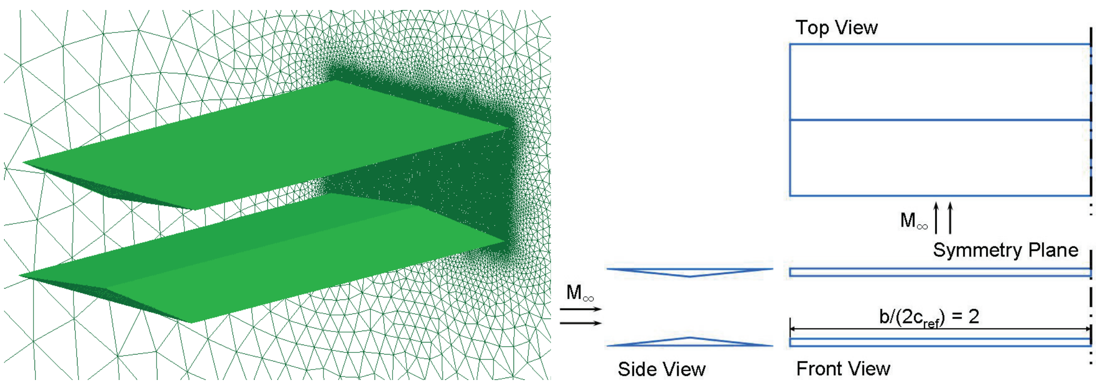

Figure 6. Rectangular wing configuration and orthography drawing.

C. Winglet wing

The winglet wing configuration is a rectangular wing with a winglet at the wing tip. This wing configuration is shown in Figure 7. The winglet is added to shut out the influence of the Mach cone between two wings. The wing section configuration of the winglet is a triangle airfoil and its t/c is set to 0.01 to reduce drag as much as possible.

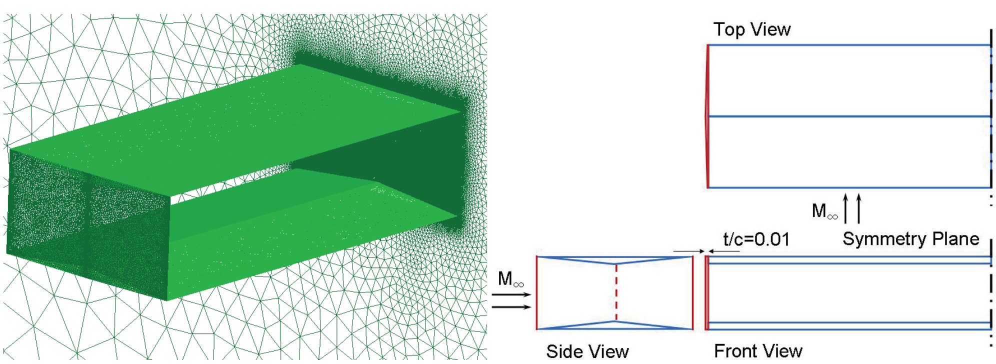

Figure 7. Winglet wing configuration and orthography drawing.

D. Caret biplane wing

The Caret biplane wing based on the Caret wing is shown in Figure 8. This wing configuration is based on the Caret wing proposed for Waverider.[9] The original Caret wing is designed to create a planar shock wave attached at the leading edge. The Caret wing configuration is shown in Figure 9. Caret biplane wing is designed for not creating a Mach cone at the wing root. Caret biplane wing is divided three regions. From the leading edge, the first region is a compression region, the second region is a no compression and no expansion region and the third region is an expansion region. This compression region is the Caret wing configuration. No compression and no expansion region is for a shock wave interaction. The airfoil of this wing section is a trapezoid only in this case. This airfoil thickness-chord ratio is 0.0357 and wedge angle (ε) is 5.71 degrees. The wing span is 4 (b/c = 2). Then, the dihedral angle is 17.72 degrees.

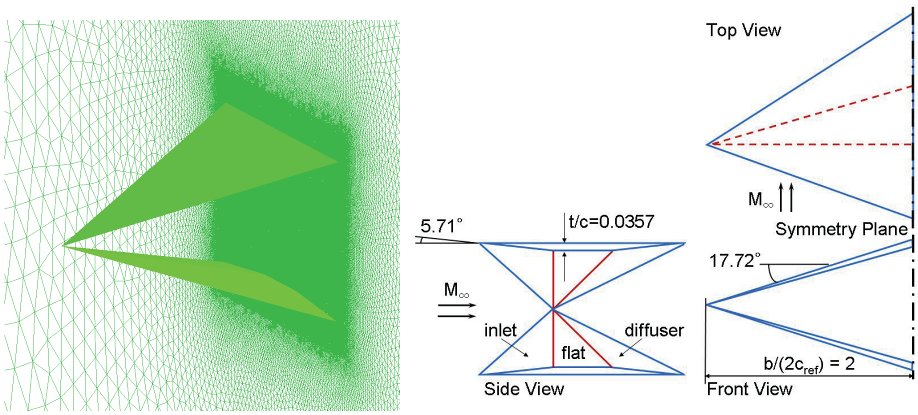

Figure 8. Caret biplane wing configuration and orthography drawing.

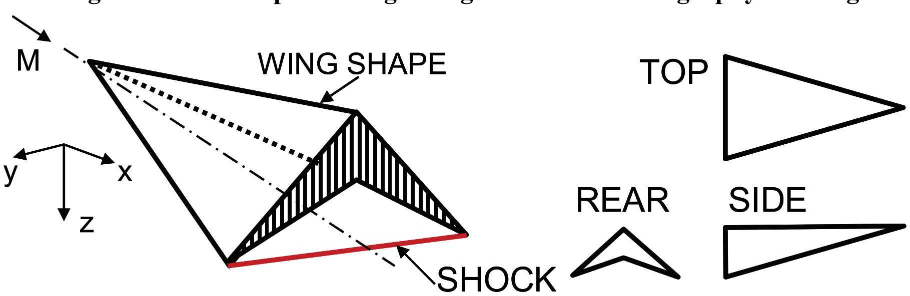

Figure 9. Caret wing configuration and orthography drawing.

E. Trailing-edge tapered wing

The trailing-edge tapered wing configuration is only the trailing-edge tapered. The taper is set to reduce the area affected by Mach cones near the wing tip. And each wing has a dihedral to keep a favorable shock wave interaction at each wing section. The tapered wing used in this study is shown in Figure 10. The taper ratio is 0.4. The dihedral angle is 6.18 degrees.

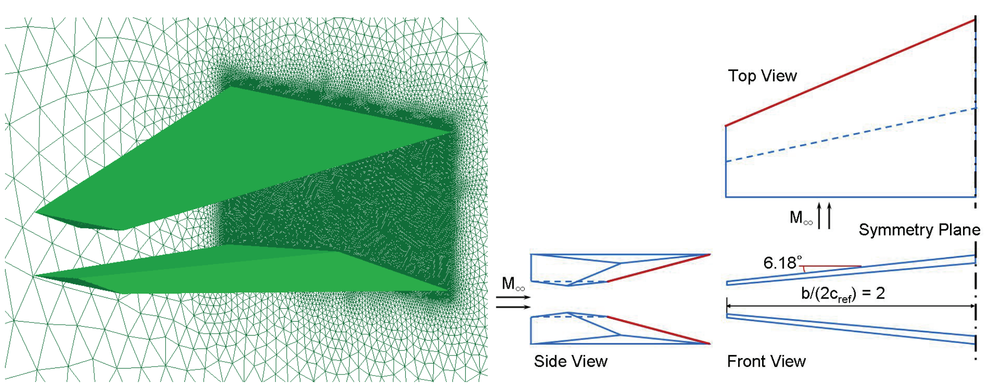

Figure 10. Trailing-edge tapered wing configuration.

F. Leading-edge and trailing-edge tapered wing

The leading-edge and trailing-edge tapered wing configuration is shown in Figure 11. This wing is tapered at both the leading edge and the trailing edge. This wing designed shut out the influence of the Mach cone between two wings by using a taper. The wing span is 4 (b/c = 2). The dihedral angle is 10.42 degrees.

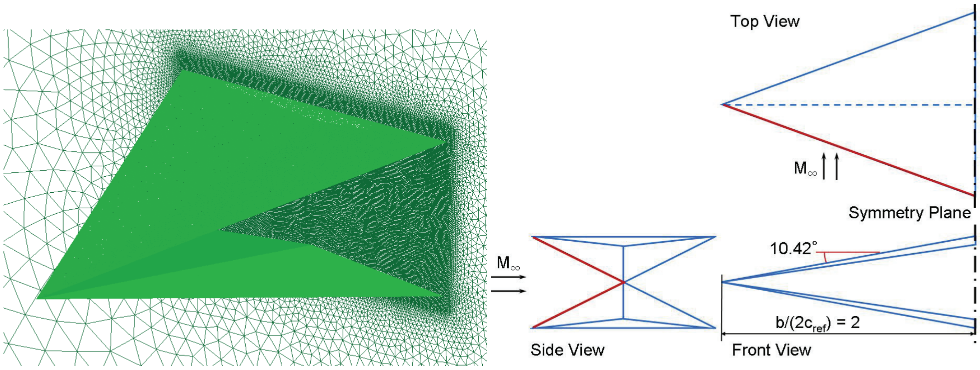

Figure 11. Leading-edge and trailing-edge tapered wing configuration.

IV. Results and Discussion

Rectangular wing

Figure 12 shows the C_p contour plots around wing sections at y/c = 1.0 and 1.8 and on the wing surface of the shock wave interaction side. The C_p contour at y/c = 1.0 is same with the two-dimensional result. But the C_p contour at y/c = 1.8 is different from the two-dimensional result. The area in which the pressure on the front region from the vertex of the wing section is identical to that of the back region (like the areas from y/c = 0 to 1.1 in Figure 12 (c)) maintains the two-dimensionality. And two Mach cones appear from the leading-edge and vertex at the wing tip (see in Figure 12 (c)). This is the three-dimensional effect. Figure 12 (c) shows that the shock wave interaction is disturbed by these Mach cones because these Mach cones are expansion waves and overlap with the shock wave interaction. By influence of these Mach cones, the area into the Mach cones has the drag coefficient increases (see in Figure 13).

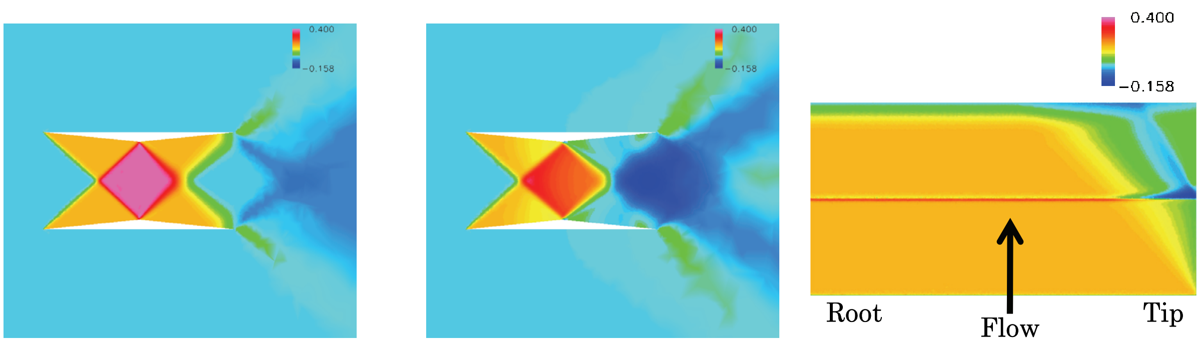

(a) At y/c = 1.0. **(b) At y/c = 1.8.** **(c) On the wing surface at interaction side.**

Figure 12. *C_p* contour plots of the rectangular wing.

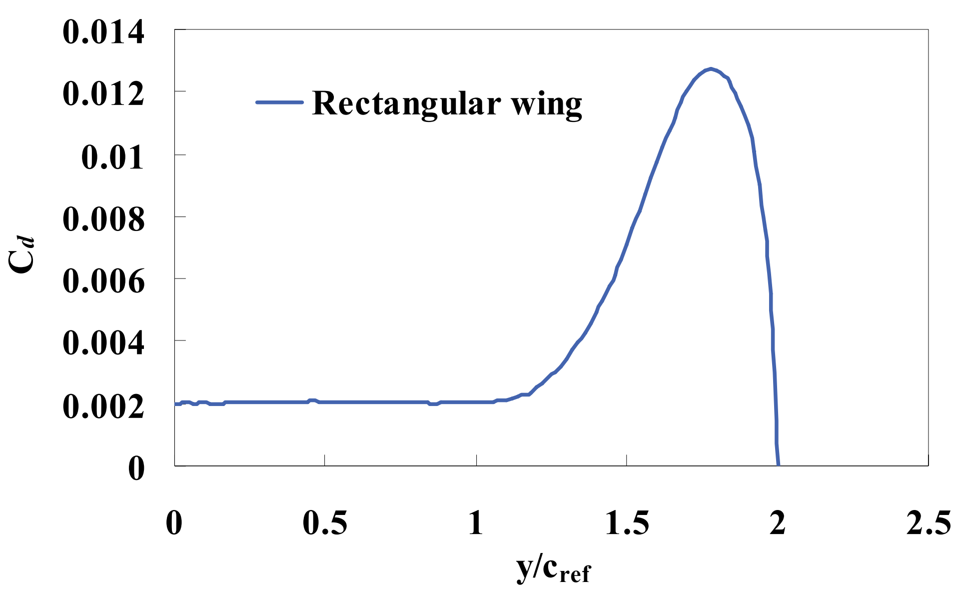

Figure 13. *C_d* distribution along the span direction of the rectangular wing.

Winglet wing

The C_p contour plot on the wing surface of the winglet wing is shown in Figure 14. The winglet wing maintains the two-dimensionality from the wing root to wing tip thanks to the winglet. As a result, C_d distribution along the span direction of the winglet wing is constant from the wing root to wing tip (see in Figure 15).

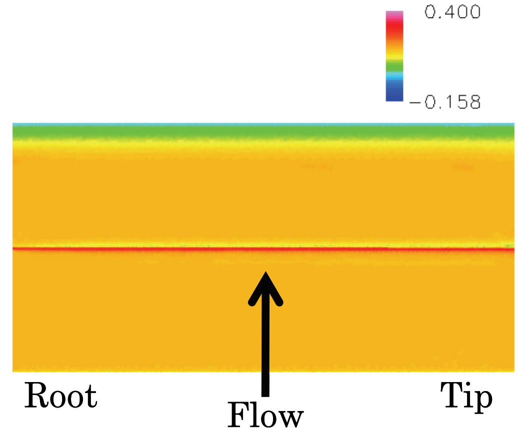

Figure 14. C_p contour plot on the wing surface at the interaction side of the winglet wing.

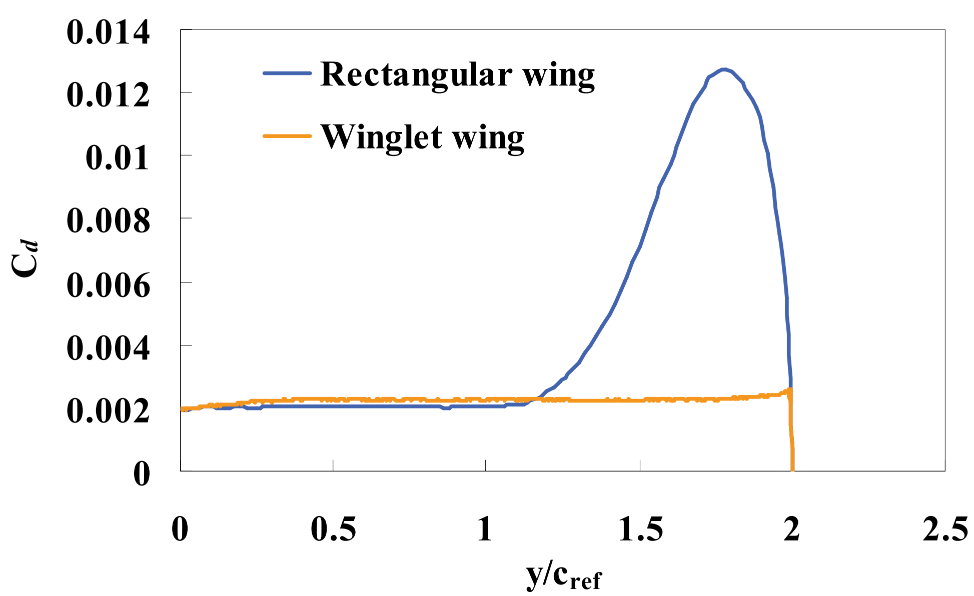

Figure 15. C_d distribution along the span direction of the winglet wing.

Caret biplane wing

The C_p contour plot around the cross section at x/c = 0.3 is shown in Figure 16. As the compression area of this wing is the Caret wing configuration, each planar shock wave attached at the leading edge (see in Figure 16). Behind the second region, Mach cones created (see in Figure 17). For this reason, the two-dimensionality cannot be maintained behind the second region. Figure 18 shows the C_p contour plot around a wing section not be influenced of these Mach cones. The low pressure area at the trailing edge is larger than that in the 2-D analysis. The pressure is further decreased due to Mach cones. As a result, C_d distribution along the span direction of the Caret biplane wing is a staged distribution (see in Figure 19).

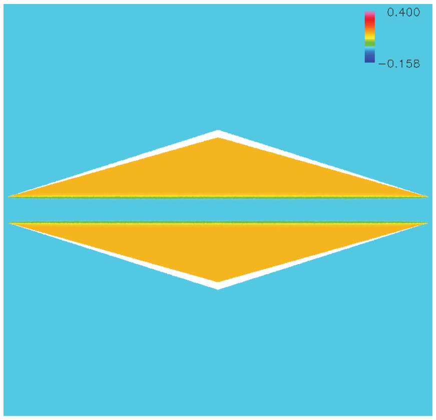

Figure 16. C_p contour plot around the cross section at x/c = 0.3.

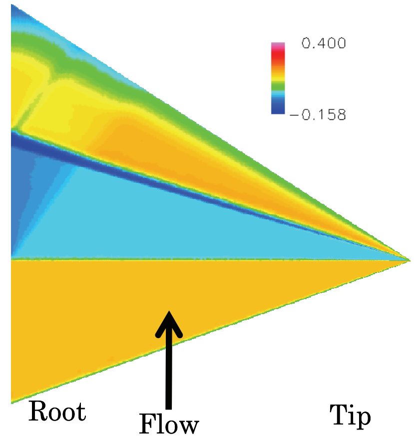

Figure 17. C_p contour plot on the wing surface at the interaction side of the Caret biplane wing.

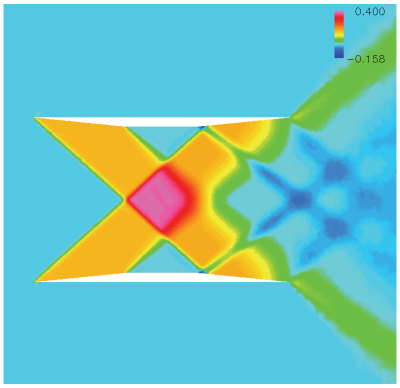

Figure 18. C_p contour plot around the wing section at y/c = 0.4.

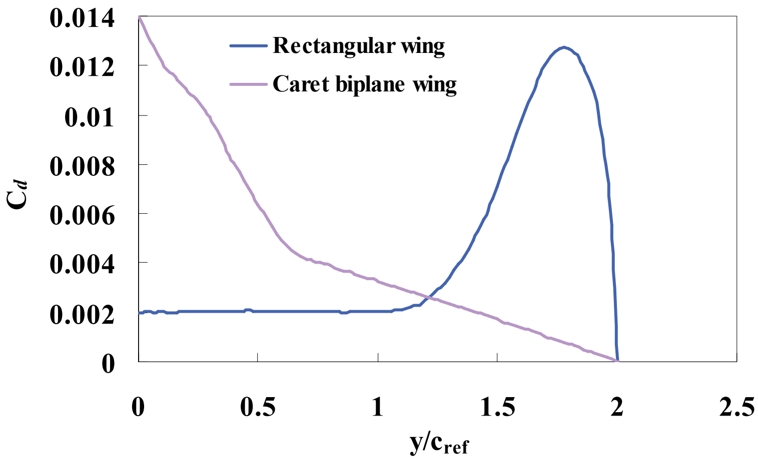

Figure 19. C_d distribution along the span direction of the Caret biplane wing.

Trailing-edge tapered wing

The C_p contour plot on the wing surface of the trailing-edge tapered wing is shown in Figure 20. This configuration creates a compression Mach cone at wing root because the shock front from the leading edge crosses the shock front from the other side wing. And the pressure on the back region from the vertex of the wing section is lower than that on the front region in the area avoiding the influence of the Mach cones (see in Figure 21). This configuration reduces drag coefficients near the wing tip because it is originally created to have relatively a small wing tip (see in Figure 22). But the drag coefficient increases at the wing root due to the compression Mach cone.

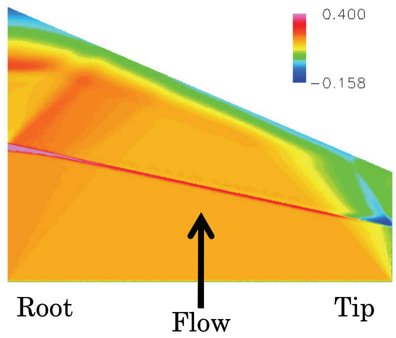

Figure 20. C_p contour plot on the wing surface at the interaction side of the trailing-edge tapered wing.

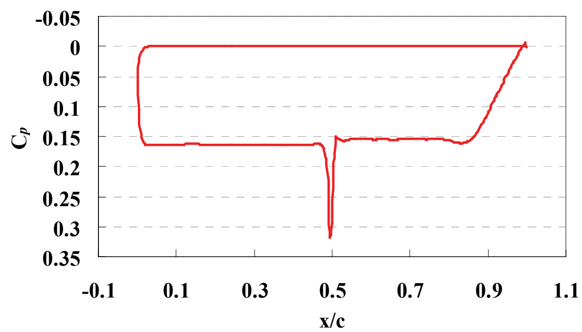

Figure 21. C_p distribution on the wing section at the y/c =1.0.

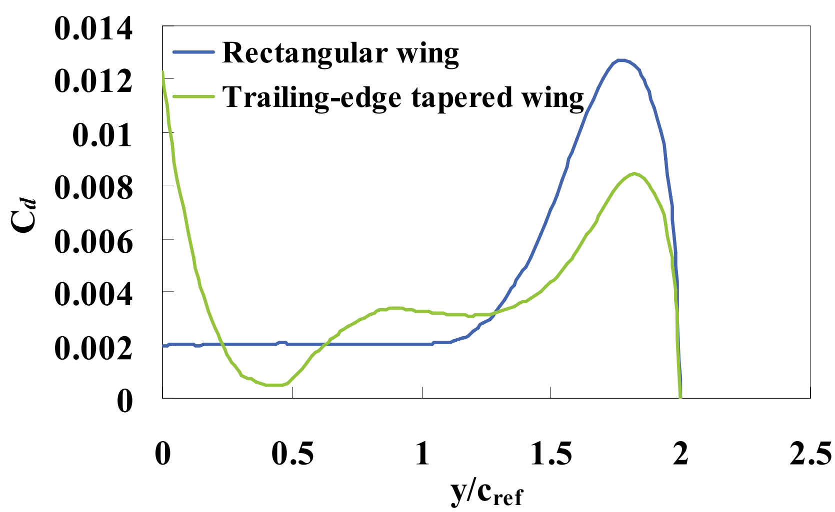

Figure 22. C_d distribution along the span direction of the trailing-edge tapered wing.

Leading-edge and trailing-edge tapered wing

The C_p contour plot on the wing surface of the leading-edge and trailing-edge tapered wing is shown in Figure 23. This configuration creates expansion Mach waves at the wing root. And the pressure on the back region from the vertex of the wing section is higher than that on the front region in the area avoiding the influence of the Mach cone (see in Figure 24). As a result, the drag coefficients are nearly zero in this area (see in Figure 25).

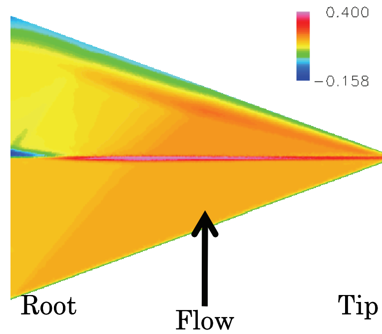

Figure 23. C_p contour plot on the wing surface at the interaction side of the leading-edge and trailing-edge tapered wing.

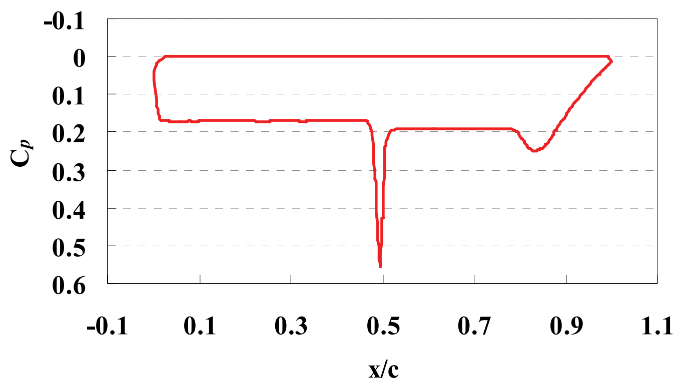

Figure 24. C_p distribution on the wing section at the y/c =1.0.

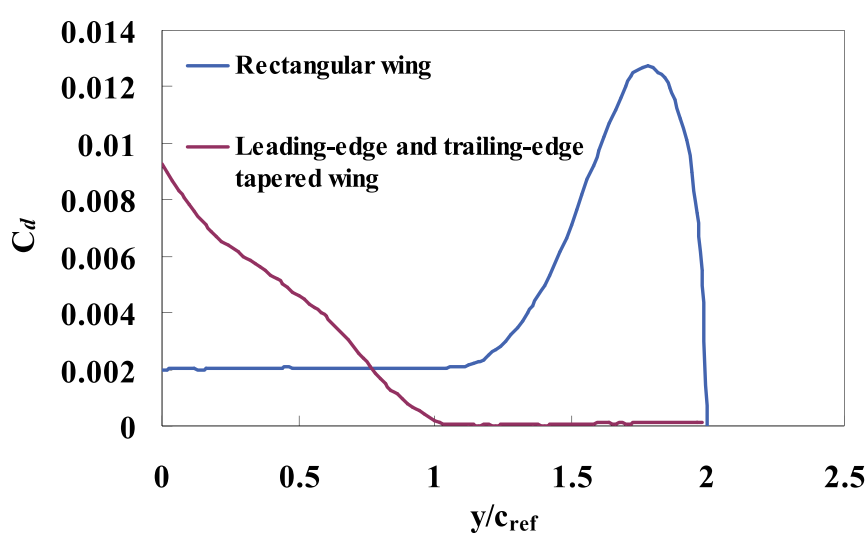

Figure 25. C_d distribution along the span direction of the leading-edge and trailing-edge tapered wing.

Comparison of total wave drag coefficient

The total wave drag coefficients of all wings in this study are tabled on the Table 1. That of the winglet wing is nearest equal that of the original airfoil. From the view points of the structure and skin friction, however, the winglet wing receives further considerations due to the winglet.

Table 1. C_D of each configuration.

Wing Configuration	C_D
Rectangular wing	0.0047
Winglet wing	0.0024
Caret biplane wing	0.0045
Trailing-edge tapered wing	0.0040
Leading-edge and trailing-edge tapered wing	0.0031
Busemann biplane airfoil	0.0020

V. Concluding Remarks

The influence of the three-dimensional effect in the Busemann biplane wing was investigated in this study. For that purpose, five typical wings using the biplane concept were analyzed for their shock wave interaction patterns.

The C_d is increased near the wing tip of the rectangular wing, because the Mach cones disturb the shock wave interaction near the wing tip.

The winglet wing can shut out the wing-tip effect. Thus, the two-dimensionality of flow is maintained within the biplane from the wing root to the wing tip, and its C_D is nearly equal to that of the Busemann biplane airfoil.

Planar shock wave can be obtained at the compression area of the Caret biplane wing. However, the Mach cones appear at the wing root in the other regions as well.

The trailing-edge tapered wing with the taper ratio of 0.4 can slightly reduce the C_D as compared to the rectangular wing. However, its C_d increases at the shock wave interaction area and the Mach cones also appear at the wing root.

The C_D of the leading-edge and trailing-edge tapered wing is not that high as compared to those of other wings. This is because the leading-edge and trailing-edge tapered wing can shut out the wing tip effect and thus its C_d decreases at the shock wave interaction area.

It can be concluded that among the five wings, the winglet wing is the best in terms of total drag coefficient, but further considerations in viscous drag, as well as the structural performance due to the large winglet, are required. The leading-edge and trailing-edge tapered wing shows the good performance in the total drag coefficient as compared to other wings in this study.

References

[1]Liepmann, H. W. and Roshko, A., *Elements of Gas Dynamics*, John Wiley & Sons, Inc., New York, 1957, pp.107-123, pp.389.

[2]Antonio, F., *Elements of Aerodynamics of Supersonic Flows*, Dover Phoenix Editions, Macmillan Company, New York, 1949, pp.154-160.

[3]Kusunose, K., Matsushima, K., Goto, Y., Yamashita, H., Yonezawa, M., Maruyama D. and Nakano T., "A Fundamental Study for the Development of Boomless Supersonic Transport Aircraft," AIAA paper 2006-0654, 2006.

[4]Ito, Y. and Nakahashi, K. "Direct Surface Triangulation Using Stereolithography(STL) Data,"AIAA paper 2000-0924, 2000.

[5]Sharov, D. and Nakahashi, K. "Hybrid Prismatic/Tetrahedral Grid Generation for Viscous Flow Applications," AIAA paper 96-2000, 1996.

[6]Ito, Y. and Nakahashi, K. "Unstructured Mesh Generation for Viscous Flow Computations," *Proceedings of the 11th International Meshing Roundtable*, Ithaca, NY, 2002, pp. 367–377.

[7]Obayashi, S. and Guruswamy, G. P. "Convergence Acceleration of an Aeroelastic Navier-Stokes Solver," *AIAA Journal*, Vol. 33, No. 6, 1994, pp. 1134–1141.

[8]Sharov, D. and Nakahashi, K. "Reordering of Hybrid Unstructured Grids for Lower-Upper Symmetric Gauss-Seidel Computations," *AIAA Journal*, Vol. 36, No. 3, 1998, pp. 484–486.

[9]Bowcutt, K., G., Anderson, J., D., and Capriotti, D., "Viscous Optimized Hypersonic Waveriders," AIAA Paper 87-0272, 1987.